applied sciences

MDPI

Article

Dynamic Coefficients of Tilting Pad Bearing by Perturbing the Turbulence Model

Dongjiang Han [1,2,*], Chunxiao Bi [1,2], Ce Chen [3] and Jinfu Yang [1,2]

[1] Institute of Engineering Thermophysics, Chinese Academy of Sciences, Beijing 100190, China; bichunxiao@iet.cn (C.B.); yangjinfu@iet.cn (J.Y.)
[2] University of Chinese Academy of Sciences, Beijing 100049, China
[3] Chinese People's Liberation Army Aviation School, Research Institute, Beijing 101121, China; cc_archer@163.com
* Correspondence: handongjiang@iet.cn

Abstract: Tilting pad bearings are appropriate for the trend of high efficiency and reliability design of rotating machinery due to their high stability. The laminar and turbulent flow states exist in the lubricating oil film of high-speed and heavy-load tilting pad bearings simultaneously. By perturbing the multiple flow state lubrication model with a partial derivative method, together with the pad-pivot structural perturbations, the frequency-dependent stiffness and damping coefficients of tilting pad bearings, embracing the effect of dynamical variations of both turbulence and pressure-viscous, were numerically solved in this research. The importance of each perturbed variable was studied, and the results indicate that the perturbed film thickness included in turbulence coefficients perturbations is significant enough to be taken into account otherwise the equivalent stiffness coefficients will be obviously overestimated. Unlike the perturbed film thickness, the consideration of the perturbed viscosity is optional, because it makes the stiffness and damping coefficients larger at both laminar and turbulent flow states. For a simplified simulation and conservative prediction results, the perturbed viscosity can be neglected.

Keywords: multiple flow state lubrication; dynamical variation effect; frequency dependence; dynamic stiffness and damping coefficients; pressure-viscous effect

check for updates

Citation: Han, D.; Bi, C.; Chen, C.; Yang, J. Dynamic Coefficients of Tilting Pad Bearing by Perturbing the Turbulence Model. *Appl. Sci.* **2022**, *12*, 6348. https://doi.org/10.3390/app12136348

Academic Editors: Tae Ho Kim and Junho Suh

Received: 14 May 2022
Accepted: 20 June 2022
Published: 22 June 2022

Publisher's Note: MDPI stays neutral with regard to jurisdictional claims in published maps and institutional affiliations.

Copyright: © 2022 by the authors. Licensee MDPI, Basel, Switzerland. This article is an open access article distributed under the terms and conditions of the Creative Commons Attribution (CC BY) license (https://creativecommons.org/licenses/by/4.0/).

1. Introduction

Tilting pad bearings have been widely applied in many kinds of rotating machines, such as gas turbines [1], compressors [2], and so on, due to their ability to improve stability [3]. Tilting pad bearings are also suitable for oil-free operations [4–6], so they have the potential for new fields such as electrical submersible pumps [7,8].

The dynamic stiffness and damping coefficients of bearings prominently affect the dynamic behavior of a rotor system [9], including critical speed and stability [10,11]. The pad assembly method was firstly established by Lund [12] for calculating the synchronous dynamic coefficients of tilting pad bearings. Lund's method requires that the excitation frequency of the pad and shaft is assumed synchronous with the shaft rotation frequency. However, the use of synchronous coefficients tends to overestimate stability, especially in the case of a high Sommerfeld number [13] so the sub-synchronous dynamic coefficients are quite important. Suh studied the effects of thermal boundary condition on the stiffness and damping coefficients for tilting pad bearings [14]. Experimental studies of tilting pad bearings also indicated the frequency dependence of dynamic coefficients [15]. Yang advanced the partial derivative method for the prediction of a complete set of dynamic coefficients of tilting pad gas bearings [16]. Though this method successfully solved the perturbation frequency effect of dynamic coefficients, it is not suitable for turbulent lubrication.

The turbulence effect on static and dynamic properties of bearings cannot be neglected in heavy loads or high rotational speeds [17]. White developed an approximate

one-dimensional finite element method for Reynolds equation with turbulence correction factors based on Hirs bulk-flow theory. Then the dynamic characteristics under half speed whirl were investigated [18]. Dousti and Allaire presented a comprehensive thermohydrodynamic model for double-film floating disk thrust bearings based on Reynolds and energy equations considering turbulence effect [19]. Lv investigated heavy-duty bearings by the transient mixed-lubrication model considering both turbulence in the large film thickness area and contact of asperities near the minimum nominal film thickness [20]. Yan developed the formula for the transition region of the turbulent lubrication model [21].

However, the dynamical effect of turbulence on stiffness and damping coefficients of high-speed tilting pad bearings was not considered in the turbulent lubrication studies above. The dynamical variations of turbulence coefficients along with the shaft vibration at different frequencies were incorporated into the methods for dynamic coefficients of fix pad bearings lubricated by organic refrigerant [22] and supercritical CO_2 [23]. In this research, by introducing the pad-pivot structural perturbations to the partial derivative method in Ref. [23], it was furthered to calculate the frequency-dependent stiffness and damping coefficients of oil-lubricated tilting pad bearings with laminar and turbulent states. Both the perturbed viscosity and the perturbed turbulence coefficients were embraced in the dynamic model of tilting pad bearings and then the importance of each perturbed variable was studied.

2. Mathematical Method

2.1. The Transient Reynolds Equation

The Reynolds equation considering variable viscosity and coexistence of laminar and turbulent flow is written below.

$$\frac{1}{R^2}\frac{\partial}{\partial\theta}\left(\frac{h^3}{k_x\mu}\frac{\partial p}{\partial\theta}\right)+\frac{\partial}{\partial z}\left(\frac{h^3}{k_z\mu}\frac{\partial p}{\partial z}\right)=\frac{\omega}{2}\frac{\partial h}{\partial\theta}+\frac{\partial h}{\partial t} \tag{1}$$

The k_x and k_z are circumferential and axial turbulence coefficients, respectively.

$$k_x=12+a_1Re^{b_1};\ k_z=12+a_2Re^{b_2} \tag{2}$$

where the local Reynolds number $Re=\rho\omega Rh/\mu$. The values of constants a_1, b_1, a_2 and b_2 in the Equation (2) are determined by flow state in the lubricating film. For turbulence ($Re>2000$), the $a_1=0.0136$, $b_1=0.900$ and $a_2=0.0043$, $b_2=0.960$ are given by the Ng-Pan turbulence model [24]. Otherwise, all the constants above are equal to zero and $k_x=k_z=12$ corresponding to laminar flow condition.

Considering $\lambda=2z/L$, $\overline{\mu}=\mu/\mu_a$, $\overline{p}=\psi^2p/\mu_a\omega$, $\psi=C_p/R$, $d=2R$, $\overline{h}=h/C_p$ and $\overline{t}=\omega t$, the dimensionless equation was obtained.

$$\frac{\partial}{\partial\theta}\left(\frac{\overline{h}^3}{k_x\overline{\mu}}\frac{\partial\overline{p}}{\partial\theta}\right)+\left(\frac{d}{L}\right)^2\frac{\partial}{\partial\lambda}\left(\frac{\overline{h}^3}{k_z\overline{\mu}}\frac{\partial\overline{p}}{\partial\lambda}\right)=\frac{1}{2}\frac{\partial\overline{h}}{\partial\theta}+\frac{\partial\overline{h}}{\partial\overline{t}} \tag{3}$$

2.2. Static and Perturbed Film Thickness for Tilting Pad Bearings

The shaft whirling and the pads tilting around the static equilibrium position at small amplitude can be described by perturbation of eccentricity ratio, attitude angle ($\widetilde{\varepsilon}_d$, $\widetilde{\varphi}_d$) and tilting angle $\widetilde{\delta}_d$, respectively. Then the film thickness $\overline{h}$ of the lth pad of tilting pad bearing is composed of the static $\overline{h}_0$ between the shaft and the pads at equilibrium position and the perturbed film thickness $\widetilde{h}_d$ [16].

$$\overline{h}=\overline{h}_0+\widetilde{h}_de^{i\Omega\overline{t}} \tag{4}$$

$$\overline{h}_0=1-m\cos(\beta_l-\theta)+\varepsilon_0\cos(\theta-\varphi_0)+\overline{\delta}_{0_l}\sin(\beta_l-\theta) \tag{5}$$

$$\widetilde{h}_d=\overbrace{\widetilde{\varepsilon}_d\cos(\theta-\varphi_0)+\varepsilon_0\widetilde{\varphi}_d\sin(\theta-\varphi_0)}^{shaft\ whirling}+\overbrace{\widetilde{\delta}_{d_l}\sin(\beta_l-\theta)}^{pads\ tilting} \tag{6}$$

where the β_l is the circumferential angle of the pivot position of the lth pad, as shown in Figure 1, and the subscript _l in the $\overline{\delta}_0$, $\widetilde{\delta}_d$ represents the lth pad as well. The preload factor $m = 1 - C_b/C_p$ and the $\overline{\delta} = \delta/\psi$. The dimensionless perturbation frequency Ω is the ratio of shaft perturbation frequency v to the rotating frequency ω.

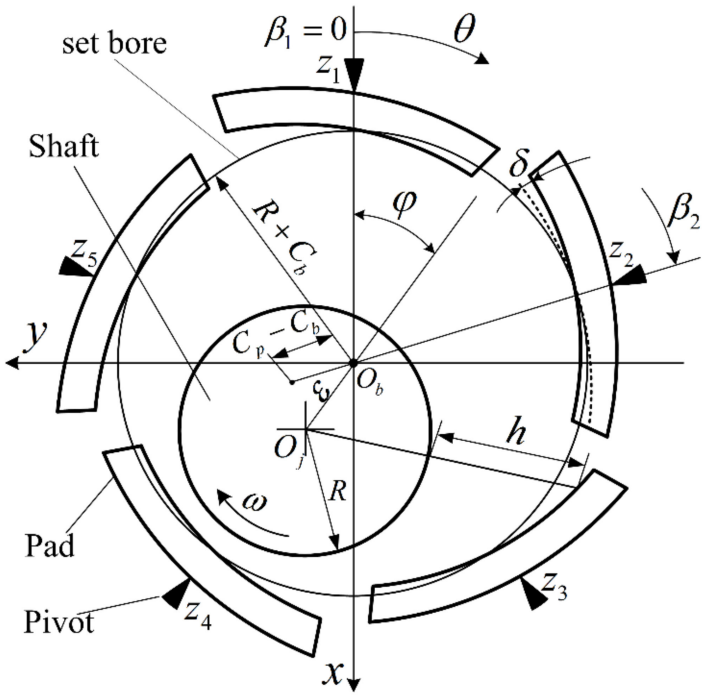


Figure 1. Schematic of tilting pad bearing (load between pad).

2.3. Static and Perturbed Reynolds Equation

With the shaft and pads perturbation, the pressure is expressed as static pressure $\overline{p}_0$ and complex perturbed pressure $\widetilde{p}_d$.

$$\overline{p} = \overline{p}_0 + \widetilde{p}_d e^{i\Omega\overline{t}} \tag{7}$$

The partial derivative method was extended in [23] embracing dynamic variations of complete variables. For the lubricating oil film, the dynamic variation of both film thickness and viscosity originate from turbulence coefficients k_x, k_z as well as $\overline{h}^3/\overline{\mu}$. The linearized complex perturbation expansions of turbulence coefficients are combined responses to perturbed film thickness $\widetilde{h}_d$ and perturbed viscosity $\widetilde{\mu}_d$.

$$\begin{aligned} \frac{1}{k_x} &= \frac{1}{k_{x0}}\left(1 + b_1\left(\frac{\widetilde{\mu}_d}{\overline{\mu}_0} - \frac{\widetilde{h}_d}{\overline{h}_0}\right)e^{i\Omega\overline{t}}\right) \\ \frac{1}{k_z} &= \frac{1}{k_{z0}}\left(1 + b_2\left(\frac{\widetilde{\mu}_d}{\overline{\mu}_0} - \frac{\widetilde{h}_d}{\overline{h}_0}\right)e^{i\Omega\overline{t}}\right) \end{aligned} \tag{8}$$

where k_{x0} and k_{z0} are static turbulence coefficients at the equilibrium position. When the $Re < 2000$, the $k_{x0} = k_{z0} = 12$ for the laminar state and the corresponding b_1 and b_2 in Equation (8) are equal to zero.

$$\begin{aligned} k_{x0} &= 12 + a_1\left(Re_c\frac{\overline{h}_0}{\overline{\mu}_0}\right)^{b_1} \\ k_{z0} &= 12 + a_2\left(Re_c\frac{\overline{h}_0}{\overline{\mu}_0}\right)^{b_2} \end{aligned} \tag{9}$$

where the $Re_c = \rho\omega RC_p/\mu_a$ is the average Reynolds number.

The relation between perturbed viscosity $\widetilde{\mu}_d$ and perturbed pressure $\widetilde{p}_d$ was constructed through a dynamic mapping [23] expressed by the dimensionless partial derivative of viscosity to pressure at $\overline{p}_0$.

$$\overline{\mu} = \overline{\mu}_0 + \widetilde{\mu}_d e^{i\Omega\overline{t}} = \overline{\mu}_0 + \overline{\partial}_{\overline{p}}\overline{\mu}(p_0, T)\widetilde{p}_d e^{i\Omega\overline{t}} \tag{10}$$

Taking Equations (4), (7), (8) and (10) into Equation (3), the static and perturbed Reynolds equation is separated, which method of derivation and solution was verified in [23].

$$\frac{\partial}{\partial\theta}\left(\frac{\overline{h}_0^3}{k_{x0}\overline{\mu}_0}\frac{\partial\overline{p}_0}{\partial\theta}\right) + \left(\frac{d}{L}\right)^2\frac{\partial}{\partial\lambda}\left(\frac{\overline{h}_0^3}{k_{z0}\overline{\mu}_0}\frac{\partial\overline{p}_0}{\partial\lambda}\right) = \frac{1}{2}\frac{\partial\overline{h}_0}{\partial\theta} \tag{11}$$

$$\begin{aligned}\frac{\partial}{\partial\theta}\left(\frac{\overline{h}_0^3}{k_{x0}\overline{\mu}_0}\frac{\partial\widetilde{p}_d}{\partial\theta}\right) &+\left(\frac{d}{L}\right)^2\frac{\partial}{\partial\lambda}\left(\frac{\overline{h}_0^3}{k_{z0}\overline{\mu}_0}\frac{\partial\widetilde{p}_d}{\partial\lambda}\right)\\ &+(b_1-1)\frac{\partial}{\partial\theta}\left(\frac{\overline{\partial}_{\overline{p}}\overline{\mu}(p_0,T)}{\overline{\mu}_0}\frac{\overline{h}_0^3}{k_{x0}\overline{\mu}_0}\frac{\partial\overline{p}_0}{\partial\theta}\widetilde{p}_d\right)\\ &+(b_2-1)\left(\frac{d}{L}\right)^2\frac{\partial}{\partial\lambda}\left(\frac{\overline{\partial}_{\overline{p}}\overline{\mu}(p_0,T)}{\overline{\mu}_0}\frac{\overline{h}_0^3}{k_{z0}\overline{\mu}_0}\frac{\partial\overline{p}_0}{\partial\lambda}\widetilde{p}_d\right)\\ &=(b_1-3)\frac{\partial}{\partial\theta}\left(\frac{\overline{h}_0^2}{k_{x0}\overline{\mu}_0}\frac{\partial\overline{p}_0}{\partial\theta}\widetilde{h}_d\right)\\ &+(b_2-3)\left(\frac{d}{L}\right)^2\frac{\partial}{\partial\lambda}\left(\frac{\overline{h}_0^2}{k_{z0}\overline{\mu}_0}\frac{\partial\overline{p}_0}{\partial\lambda}\widetilde{h}_d\right)+\frac{1}{2}\frac{\partial\widetilde{h}_d}{\partial\theta}+i\Omega\widetilde{h}_d\end{aligned} \tag{12}$$

The static Reynolds equation Equation (11) governs the static pressure $\overline{p}_0$. The perturbed equation Equation (12) is for solving the dynamic coefficients by means of a partial derivative method [16,23]. The boundary conditions of Equations (11) and (12) for oil-lubricated tilting pad bearings are shown in Equations (13)–(15). The oil is not able to bear the tensile stress. For both static and perturbed equations, the ambient pressure at two axial ends and the leading edge, and trailing edge of the pads is set at zero.

$$\overline{p}_0(\theta, \lambda = \pm 1) = \widetilde{p}_d(\theta, \lambda = \pm 1) = 0 \tag{13}$$

$$\begin{aligned}\overline{p}_0(\theta = \theta_L, \lambda) = \overline{p}_0(\theta = \theta_T, \lambda) = 0\\ \widetilde{p}_d(\theta = \theta_L, \lambda) = \widetilde{p}_d(\theta = \theta_T, \lambda) = 0\end{aligned} \tag{14}$$

When a trend of negative pressure occurs in the pads of bearing, the oil film breaks and the cavitation occurs. It is governed by the Reynolds boundary condition in this research shown as Equation (15). The static and perturbed pressure become zero at the fracture area of the oil film.

$$\begin{aligned}\overline{p}_0(\theta, \lambda) = 0\\ \widetilde{p}_d(\theta, \lambda) = 0\end{aligned} \quad if \quad \overline{p}_{0_trend}(\theta, \lambda) < 0 \tag{15}$$

2.4. The Dynamic Coefficients of Tilting Pad Bearings

For tilting pad bearings, without considering the radial displacement of pivot, the perturbation variables $\widetilde{\varepsilon}_d$, $\widetilde{\varphi}_d$ and $\widetilde{\delta}_d$ are involved in perturbed equation Equation (12). Taking partial derivative of Equation (12) to $\widetilde{\varepsilon}_d$, $\varepsilon_0\widetilde{\varphi}_d$ and $\widetilde{\delta}_d$ yields three partial differential equations for P_ε, P_φ and P_δ instead of $\widetilde{p}_d$. Meanwhile, according to Equation (6) the corresponding $\widetilde{h}_d$ is replaced by $H_\varepsilon = \cos(\theta - \varphi_0)$, $H_\varphi = \sin(\theta - \varphi_0)$ and $H_\delta = \sin(\beta_l - \theta)$, respectively. Then the numerical integration below is suitable for the coordinate system in Figure 1.

$$\begin{aligned}-\tfrac{1}{2}\int_{-1}^{1}\int_{\theta_L}^{\theta_T} P_{\bullet_l}\cos\theta d\theta d\lambda = k_{x\bullet_l} + i\Omega c_{x\bullet_l}\\ -\tfrac{1}{2}\int_{-1}^{1}\int_{\theta_L}^{\theta_T} P_{\bullet_l}\sin\theta d\theta d\lambda = k_{y\bullet_l} + i\Omega c_{y\bullet_l}\end{aligned} \tag{16}$$

where the subscript $\cdot$ represents ε, φ, and δ. The leading edge of the lth pad θ_L has a relation with pivot offset γ, pad's angular extent θ_{pad}, and β_l as $\theta_L = \beta_l - \gamma\theta_{pad}$. The relation between the lth pad's trailing edge θ_T and its leading edge θ_L is $\theta_T = \theta_L + \theta_{pad}$.

Equation (17) is employed to get dimensionless dynamic coefficients caused by shaft whirling in the coordinate system in Figure 1.

$$\begin{gathered}\begin{bmatrix} k_{xx_l} \\ k_{xy_l} \end{bmatrix} = \mathbf{A_T}\begin{bmatrix} k_{x\varepsilon_l} \\ k_{x\varphi_l} \end{bmatrix} = \begin{bmatrix} \cos\varphi_0 & -\sin\varphi_0 \\ \sin\varphi_0 & \cos\varphi_0 \end{bmatrix}\begin{bmatrix} k_{x\varepsilon_l} \\ k_{x\varphi_l} \end{bmatrix} \\ \begin{bmatrix} k_{yx_l} \\ k_{yy_l} \end{bmatrix} = \mathbf{A_T}\begin{bmatrix} k_{y\varepsilon_l} \\ k_{y\varphi_l} \end{bmatrix}; \begin{bmatrix} c_{xx_l} \\ c_{xy_l} \end{bmatrix} = \mathbf{A_T}\begin{bmatrix} c_{x\varepsilon_l} \\ c_{x\varphi_l} \end{bmatrix}; \begin{bmatrix} c_{yx_l} \\ c_{yy_l} \end{bmatrix} = \mathbf{A_T}\begin{bmatrix} c_{y\varepsilon_l} \\ c_{y\varphi_l} \end{bmatrix}\end{gathered} \tag{17}$$

The dimensionless dynamic equation of the pad corresponding to moment to the pivot is

$$\overline{J}\ddot{\overline{\delta}}_{d_l} = \overline{F}_{y_l}\cos\beta_l - \overline{F}_{x_l}\sin\beta_l \tag{18}$$

The subsequent process for deriving the dimensionless equivalent dynamic coefficients of the tilting pad bearing K_{ij} and C_{ij} ($I, j = x, y$) is similar to [16]. The dimensionless definition form is taken as [25].

$$\begin{aligned} K_{ij} &= \frac{\mu_a\omega RL}{W\psi^2}\sum_{l=1}^{5} k_{ij_l} - p\left(k_{i\delta_l}k_{\delta j_l} - \Omega^2 c_{i\delta_l}c_{\delta j_l}\right) - \Omega^2 q\left(k_{i\delta_l}c_{\delta j_l} + k_{\delta j_l}c_{i\delta_l}\right) \\ C_{ij} &= \frac{\mu_a\omega RL}{W\psi^2}\sum_{l=1}^{5} c_{ij_l} - p\left(k_{i\delta_l}c_{\delta j_l} + k_{\delta j_l}c_{i\delta_l}\right) - \Omega^2 q\left(c_{i\delta_l}c_{\delta j_l} - \frac{k_{i\delta_l}k_{\delta j_l}}{\Omega^2}\right) \end{aligned} \tag{19}$$

where

$$p = \frac{k_{\delta\delta_l} - \overline{J}\Omega^2}{\left(k_{\delta\delta_l} - \overline{J}\Omega^2\right)^2 + \left(\Omega c_{\delta\delta_l}\right)^2};\ q = \frac{c_{\delta\delta_l}}{\left(k_{\delta\delta_l} - \overline{J}\Omega^2\right)^2 + \left(\Omega c_{\delta\delta_l}\right)^2} \tag{20}$$

The pad-shaft coupling dynamic coefficients of the lth pad in Equations (19) and (20) can be obtained according to the dynamic equation of pad moment to the pivot.

$$\begin{aligned} k_{\delta x_l} &= k_{xx_l}\sin\beta_l - k_{yx_l}\cos\beta_l \\ c_{\delta x_l} &= c_{xx_l}\sin\beta_l - c_{yx_l}\cos\beta_l \\ k_{\delta y_l} &= k_{xy_l}\sin\beta_l - k_{yy_l}\cos\beta_l \\ c_{\delta y_l} &= c_{xy_l}\sin\beta_l - c_{yy_l}\cos\beta_l \\ k_{\delta\delta_l} &= k_{x\delta_l}\sin\beta_l - k_{y\delta_l}\cos\beta_l \\ c_{\delta\delta_l} &= c_{x\delta_l}\sin\beta_l - c_{y\delta_l}\cos\beta_l \end{aligned} \tag{21}$$

The dimensional dynamic coefficients can be converted as follows (taking the x direction as an example).

$$KXX = \frac{W}{C_p}K_{xx};\ CXX = \frac{W}{\omega C_p}C_{xx} \tag{22}$$

2.5. Numerical Method and Mesh Discretization

The static equation Equation (11) was discretized into a five-point difference scheme and solved by the iterative method. The static viscosity should be updated along with every iteration step of static pressure based on the Barus pressure–viscosity relationship [26] in this research. The local Reynolds number at each node need to be calculated for identifying the flow state. At the turbulence zone of lubricating film, the coefficients k_{x0} and k_{z0} should also be calculated during the iteration of pressure $\overline{p}_0$. If the static pressure $\overline{p}_0$ lower than zero occurs at a certain node during the iteration, its value would be set as zero. When the static pressure $\overline{p}_0$ reaches converge judge Equation (23), the Reynolds boundary condition Equation (15) for $\overline{p}_0$ is satisfied.

$$\frac{\sum_{i=1}^{m}\sum_{j=1}^{n}\left|\overline{p}_{0(i,j)}^{new} - \overline{p}_{0(i,j)}^{old}\right|}{\sum_{i=1}^{m}\sum_{j=1}^{n}\left|\overline{p}_{0(i,j)}^{old}\right|} \le 10^{-5} \tag{23}$$

The solution of the static equation is repeated with the iteration of the static tilting angle δ_0 of each pad.

$$\overline{M} = \int_{-1}^{1} \int_{\theta_L}^{\theta_T} (\overline{p}_0 - 1) \sin(\beta_l - \theta) d\theta d\lambda \tag{24}$$

When the dimensionless pivoted moment $\overline{M}$ shown in Equation (24) is lower than 10^{-5}, the static tilting angle δ_0 of the lth pad at its static equilibrium position is obtained.

All the variables solved from the static function Equation (11) are essential for the perturbed Reynolds equation Equation (12). Then the complex pressure distribution P_ε, P_φ and P_δ were also solved numerically by finite difference method with over-relaxation iterative. At the node where the static pressure $\overline{p}_0$ equals zero, the values of the P_ε, P_φ and P_δ should be set as zero for satisfying the Reynolds boundary condition Equation (15). The converge judges for the P_ε, P_φ and P_δ are given by Equation (25).

$$\frac{\sum_{i=1}^{m} \sum_{j=1}^{n} \left| P_{\bullet(i,j)}^{new} - P_{\bullet(i,j)}^{old} \right|}{\sum_{i=1}^{m} \sum_{j=1}^{n} \left| P_{\bullet(i,j)}^{old} \right|} \leq 10^{-5} \tag{25}$$

where the subscript $\cdot$ represents ε, φ, and δ.

The m and n in Equations (23) and (25) are grid numbers in the circumferential and axial direction, respectively. When the number of grids of each pad is larger than 32×26, the grid independence is satisfied. That is to say, the difference between results with grids of 32×26 and 64×52 is less than 2%. In the same way, the results with residuals of 10^{-5} and 10^{-6} have a small difference.

3. The Validation of Program

The program for the static characteristic of tilting pad bearing by authors was verified in Ref. [9]. For validating the dynamic characteristic program in this research, the equivalent dynamic coefficients of an oil-lubricated tilting pad bearing with the same parameters to No. 53 calculation data in the Ref. [25] were calculated. Regarding the viscosity as constant in both static and perturbed equations and the dimensionless perturbation frequency $\Omega = 1$, the results are compared with [25] and shown together in Table 1. The difference in results is less than 5%, which verified the correctness of the dynamic coefficients program with the partial derivative method. The ε' represents the assembled eccentricity ratio of tilting pad bearing, which has relation with ε_0 as $\varepsilon_0 = \varepsilon'(1 - m)$.

Table 1. The validation of the dynamic characteristics program for the tilting pad bearings.

ε'	Constant μ and without k_x, k_z				Relative Deviation			
	K_{xx}	K_{yy}	C_{xx}	C_{yy}	K_{xx}	K_{yy}	C_{xx}	C_{yy}
0.1	14.3	13.7	18.8	18.4	0.69%	1.44%	1.05%	1.08%
0.2	8.18	6.82	9.88	8.98	1.68%	0.44%	1.20%	1.43%
0.3	6.74	4.46	7.13	5.68	1.17%	2.19%	1.66%	1.73%
0.4	6.62	3.18	5.95	3.90	0.60%	2.15%	1.65%	1.76%
0.5	7.25	2.31	5.40	2.71	0.14%	1.70%	0.92%	1.81%
0.6	8.63	1.62	5.23	1.82	0.12%	2.41%	0.76%	2.15%
0.7	11.1	1.06	5.48	1.14	0.28%	1.85%	3.52%	2.56%
0.8	15.8	0.593	6.46	0.608	0.63%	2.79%	0.78%	3.18%
0.85	20.3	0.399	7.11	0.400	2.87%	2.44%	3.49%	2.91%

4. Results and Discussion

A number of studies have carried out thermohydrodynamic lubrication studies on tilting pad bearings [27–29]. However, the isothermal method, which considers the thermal effect by average viscosity (corresponding to mean temperature) of the oil film estimated from the overall heat balance [25], is still widely used for design purposes [30–32]. Such is

introduced to advanced rotor dynamics software such as Ref. [33]. In this paper, we focus on the influence of dynamical variation of turbulence coefficients and viscosity on stiffness and damping coefficients. Thus, the lubricating film is considered isothermal. For the same reason, the impact of inertia of the pad is not considered. So the cross-coupling equivalent stiffness and damping coefficients of tilting pad bearing are close to zero.

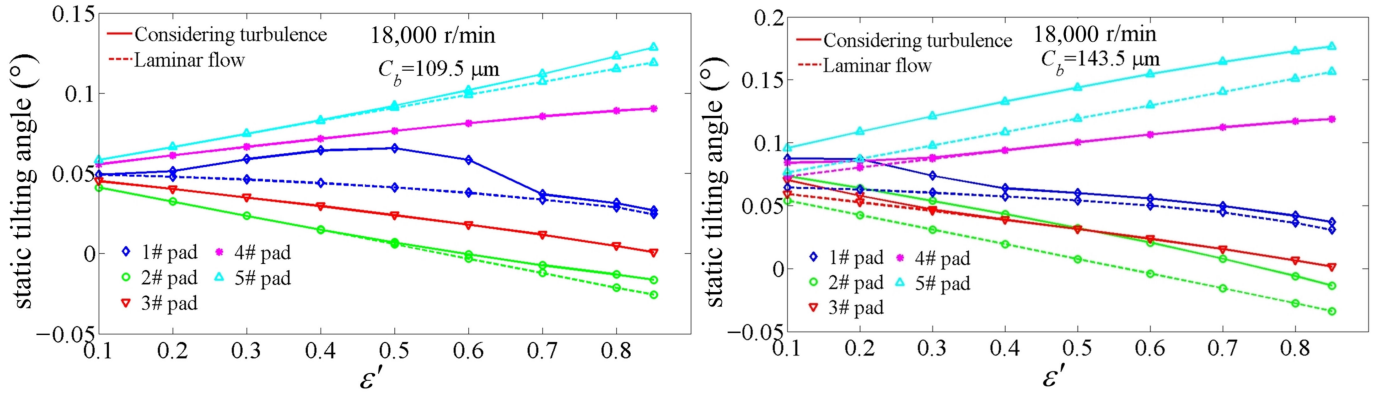
The structure and operating parameters of the tilting pad bearing are shown in Table 2 unless otherwise stated, and the assembled radius clearance C_b has values of 109.5 and 143.5 μm which were taken from a rotor system of a certain modeled gas turbine test rig.

Table 2. Parameters of tilting pad bearing.

Parameters	Value
Bearing radius (R)	70 mm
Bearing length (L)	56 mm
Pad arc angle (α)	60°
Preload factor (m)	0.5
Pivot offset (γ)	0.5
Density of lubrication oil (ρ)	871 kg/m^3
Average viscosity of oil film (μ_a)	9.37 mPa·s

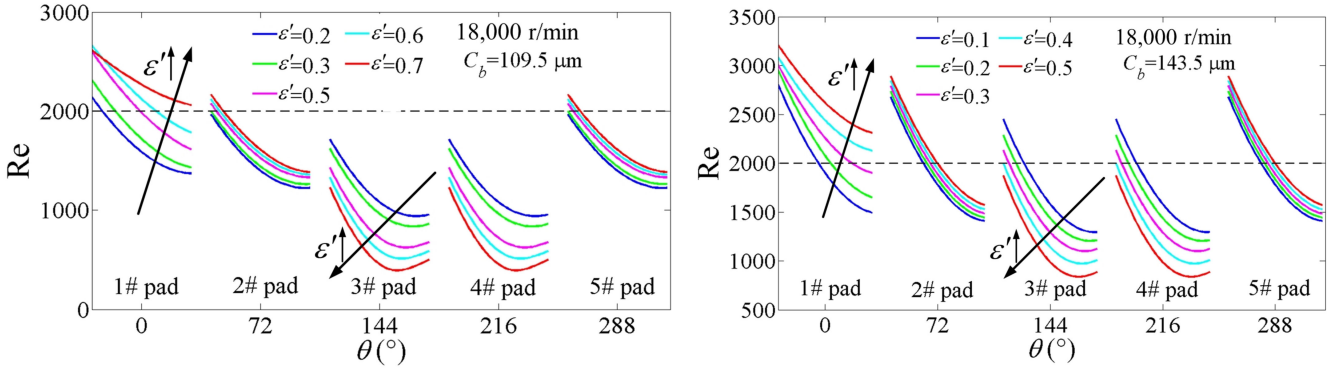
4.1. Analysis of Coexistence of Laminar and Turbulent Flow

Figure 2 shows the changes in the static tilting angle of each pad (in degree) of tilting pad bearing with assembled eccentricity ratio ε' at a rotating speed of 18,000 r/min. With the increase of ε', the tilting angle of both the 5# pad and the 4# loaded pad increases, and that of the 2# pad and 3# loaded pad decreases. The results obtained by the model considering turbulence and the pure laminar model were compared. The corresponding distributions of the local Reynolds number of each pad are shown in Figure 3. The larger the ε' is, the lower the local Reynolds number Re of oil film of 3# and 4# loaded pads are, and the higher the Re of other pads are. The reason is that a larger ε' makes a closer distance between the shaft and loaded pads, which means a smaller oil film thickness of loaded pads.



(**a**) C_b = 109.5 μm (**b**) C_b = 143.5 μm

Figure 2. Changes of the static tilting angle of each pad of tilting pad bearing with assembled eccentricity ratio at different assembled clearance.



(**a**) C_b = 109.5 μm (**b**) C_b = 143.5 μm

Figure 3. Distributions of the local Reynolds number of each pad of tilting pad bearing at different assembled eccentricity ratios and assembled clearances.

For C_b = 109.5 μm, the flow state in all the pads is laminar at $\varepsilon' = 0.1$. When the ε' increases, turbulence appears in the upper reaches of the 1# top pad (see Figure 3a), which makes the tilting angle of the 1# pad larger (see Figure 2a) because the turbulence in the upper reaches increases the oil film force. However, the difference between the tilting angle of the 1# top pad obtained by the model considering turbulence and the pure laminar model increases first and then decreases at ε' beyond 0.5 because the proportion of turbulence zone of the 1# pad becomes larger than pivot offset and the turbulence existed also in pivot downstream. When the ε' increases to 0.7, flow in the whole oil film of the 1# pad is turbulent, so the influence of turbulence on its tilting angle becomes weak. The flow state in the 3# and 4# loaded pads is laminar at arbitrary ε' for C_b = 109.5 μm. The tilting angle of both the 2# and the 5# pad obtained by the model considering turbulence becomes larger than that by the pure laminar model when ε' is over 0.6 because turbulence appears in the upper reaches of the oil film of 2# and 5# pad.

The relation between the tilting angle of the five pads for C_b = 143.5 μm has some difference to smaller assembled radius clearance when the coexistence of laminar and turbulent flow is considered. The turbulence in the 2# pad makes its static tilting angle close to that of the 3# pad. The proportion of turbulence zone of the upper reaches of both the 2# and the 5# pad is about equal to pivot offset at arbitrary ε' (see Figure 3b), so the turbulence effect increases their tilting angle obviously (see Figure 2b). The flow state in all the pads contains laminar and turbulence together at $\varepsilon' = 0.1$, 0.2, and 0.3. When the ε' increases to 0.4, the flow state in the 3# and 4# loaded pads become pure laminar flow. The influence of turbulence on the tilting angle of the 3# and 4# pads is also not very obvious at small ε' because their lubricating film is thin. The turbulence exists in the 1#, 2#, and 5# pads at arbitrary ε'. The influence of turbulence on the tilting angle of the 1# pad is weak at ε' larger than 0.4, the reason for which is the same as that of C_b = 109.5 μm at ε' larger than 0.7.

4.2. The Influence of the Perturbed Viscosity on Dynamic Coefficients

Figure 4 illustrates the dimensionless equivalent dynamic coefficients with the change of ε' for different assembled clearance C_b. The difference between results obtained by the model considering turbulence and the pure laminar model is compared, and the influence of perturbed viscosity was also investigated.

For either the model considering turbulence or the pure laminar model, each dimensionless stiffness or damping coefficient considering perturbed viscosity is larger than that without perturbed viscosity. Especially the stiffness coefficients and damping coefficients C_{xx} for C_b = 109.5 μm at ε' larger than 0.7 (see Figure 4a,c,e), the influence of perturbed viscosity is notably obvious. A reason is that the smaller oil film thickness of the 3# and 4# loaded pads enhances the pressure-viscous effect.

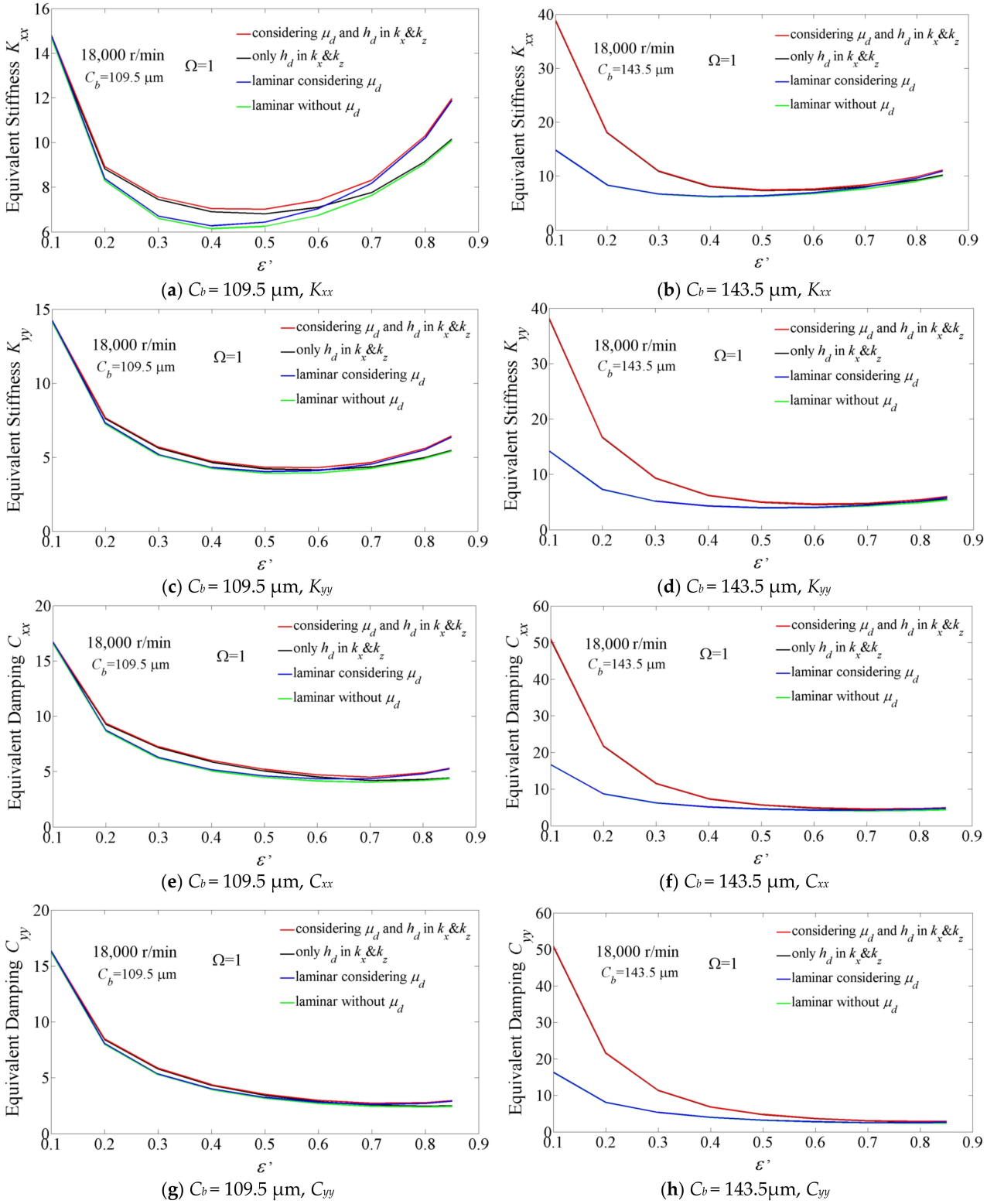


Figure 4. Changes of the dimensionless equivalent dynamic coefficients with assembled eccentricity ratio at different assembled clearance.

For C_b = 109.5 μm, with the increase of ε', the difference between results obtained by the model considering turbulence and the pure laminar model increases first and then declines after about ε' = 0.4. Such is corresponding to the local Reynolds number (see Figure 3a) and the turbulence influence on the tilting angle of the 1# top pad (see Figure 2a).

For C_b = 143.5 μm, both the dimensionless equivalent stiffness coefficients and the damping coefficients considering turbulence are prominently larger than that obtained by the pure laminar model at ε' = 0.1, 0.2, and 0.3, which reason is that the upper reaches of the oil film of 3# and 4# pads are in a turbulent state. When the ε' is larger than 0.4, the difference between results obtained by the two models becomes small and decreases gently with ε'. A reason is that the flow state in the whole oil film of the 1# top pad is turbulent (see Figure 3b) and the influence of turbulence on the tilting angle of the 1# pad is weak (see Figure 2b). The turbulence has nearly no effect on dimensionless dynamic coefficients at large ε' though the oil film of 2# and 5# pads contains both laminar and turbulent flow because the oil film thickness of the 3# and 4# loaded pads is small and the viscous effect is dominant.

4.3. The Influence of Perturbed Film Thickness Included in Turbulence Coefficients

For assembled radius clearance C_b = 143.5 μm and at assembled eccentricity ratio ε' = 0.1, the variations of dimensionless equivalent dynamic coefficients of a tilting pad bearing with rotating speed under dimensionless perturbation frequency Ω = 0.5 and 1 are shown in Figure 5. Various kinds of solving situations were presented together for reflecting the contributions of perturbed film thickness included in turbulence coefficients perturbation. The results shown in red and black lines were obtained by the partial derivative method embracing turbulence perturbation. Though the turbulence was considered in the results shown in the blue line, the influence of dynamical variation of turbulence coefficients is not considered.

Comparison of red (or black) line to blue line indicates that neglecting the perturbed film thickness $\widetilde{h}_d$ included in turbulence coefficients perturbation k_x, k_z leads to obviously excessive results of equivalent stiffness coefficients at rotating speed beyond a certain value. Under different dimensionless perturbation frequencies Ω, the regulation of the influence of turbulence perturbation on a certain stiffness or damping coefficient is similar.

The dimensionless equivalent stiffness coefficients under dimensionless perturbation frequency Ω = 0.5 are larger than that under Ω = 1. However, the dimensionless equivalent damping coefficients present the opposite relationship. Under different Ω, the variation regulation of each dynamic coefficient with rotating speed is consistent.

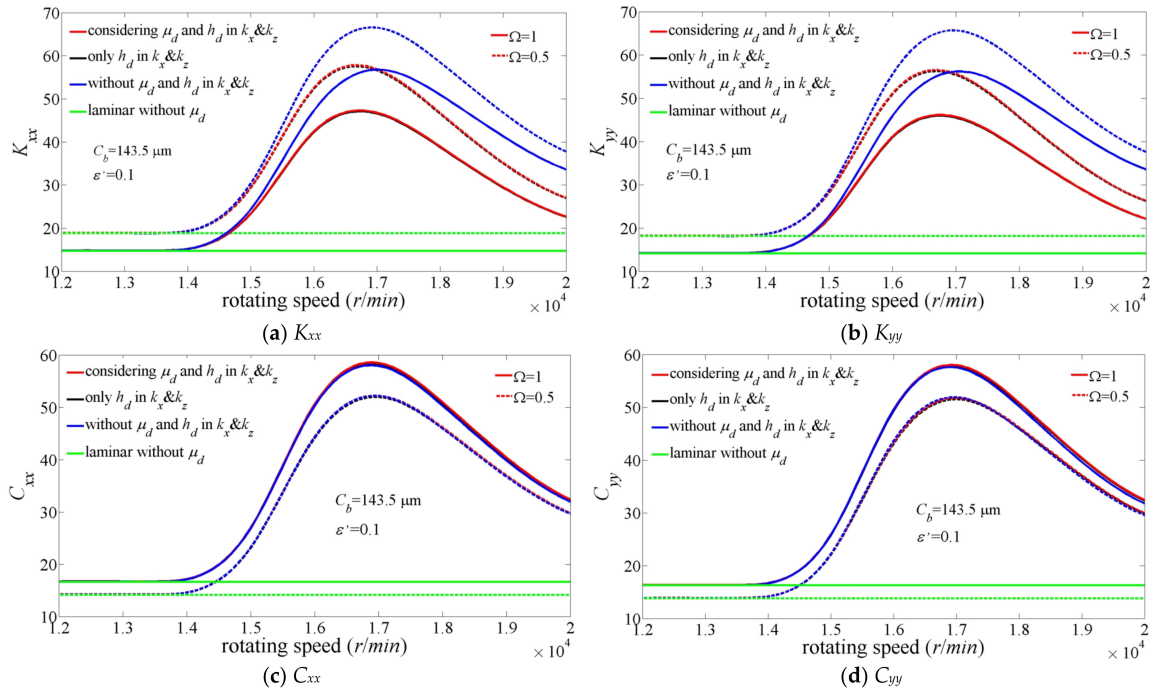


Figure 5. Variations of the dimensionless equivalent dynamic coefficients with rotating speed at assembled clearance C_b = 143.5 μm.

5. Conclusions

For studying the dynamical effect of turbulence on frequency-dependent stiffness and damping coefficients of high-speed oil-lubricated tilting pad bearings, the partial derivative method was used for perturbing the turbulent lubrication model. In this research, the perturbations of both viscosity and turbulence coefficients were embraced in the dynamic model of tilting pad bearings. The importance of each perturbed variable was studied, and the main conclusions from the results are as follows:

(1) The influence of turbulence on dimensionless dynamic coefficients is obvious at a medium assembled eccentricity ratio (about 0.3 to 0.5) for small assembled radius clearance, and at a small assembled eccentricity ratio (about 0.1 to 0.3) for large assembled radius clearance. The perturbed viscosity takes effect mainly at the large assembled eccentricity ratio for small assembled radius clearance.
(2) For large assembled radius clearance and at high rotating speed, neglecting the perturbed film thickness included in turbulence coefficients perturbations will lead to obviously excessive results of equivalent stiffness coefficients. Thus, the dynamic effect of turbulence needs to be considered.
(3) The perturbed viscosity makes the stiffness and damping coefficients larger at both laminar and turbulent flow states, so the consideration of the perturbed viscosity is optional. For a simplified simulation and conservative prediction results, the perturbed viscosity can be neglected.

Author Contributions: Conceptualization, C.B. and D.H.; Methodology, C.B.; Data curation, D.H.; Formal analysis, C.C. and D.H.; Investigation, D.H.; Project administration, C.C. and D.H.; Software, C.B. and D.H.; Validation, C.B. and D.H.; Writing—original draft, C.B. and D.H.; Writing—review and editing, D.H.; Funding acquisition, D.H. and J.Y. All authors have read and agreed to the published version of the manuscript.

Funding: This work was supported by the National Science and Technology Major Project (2017-IV-0010-0047), Youth Innovation Promotion Association CAS (2021141), and the National Natural Science Foundation of China (Grant No. 11602268).

Institutional Review Board Statement: Not applicable.

Informed Consent Statement: Not applicable.

Data Availability Statement: Not applicable.

Acknowledgments: The authors wish to express their thanks to Comrade Yao WU (from Shaanxi University of Science & Technology) for his help for programming and guidance on algorithms. The authors also gratefully acknowledge the editors and reviewers for their useful suggestions and comments.

Conflicts of Interest: The authors declared no conflict of interest with respect to the research, authorship, and publication of this article.

Nomenclature

z	axial coordinate
R	bearing radius
d	bearing diameter
L	bearing length
θ	circumferential angular coordinate
λ	dimensionless axial coordinate
$\overline{h}$	dimensionless film thickness
C_p	pad/nominal radius clearance
C_b	assembled radius clearance
δ	pad's tilting angle (in radian)
emphm	preload factor
ψ	clearance ratio
$\overline{\mu}$	dimensionless viscosity

$\overline{p}$	dimensionless pressure
ω	rotational circular frequency
$\overline{t}$	dimensionless time
ε	eccentricity ratio
φ	attitude angle
ε'	assembled eccentricity ratio
$\overline{F}_x$, $\overline{F}_y$	dimensionless dynamic oil-film forces in the x-y Cartesian coordinate
v	shaft perturbation circular frequency
Ω	dimensionless perturbation frequency
k_x, k_z	turbulence coefficients
a_1, b_1, a_2, b_2	constants in the turbulence coefficients
μ_a	average viscosity
β_l	circumferential angular location of the pivot of the lth pad (l = 1, 2, . . . , 5)
α	pad arc angle (in degree)
θ_{pad}	pad's angular extent (in radian)
γ	pivot offset
θ_L	pad's leading edge
θ_T	pad's trailing edge
$\overline{J}$	dimensionless pad moment of inertia
W	static load of the bearing
Subscripts	
0	static variables
d	perturbations
l or $_l$	the lth pad/pivot (l = 1, 2, . . . , 5)
Headers	
~	complex amplitude of frequency perturbation

References

1. Hei, D.; Lu, Y.; Zhang, Y.; Lu, Z.; Gupta, P.; Müller, N. Nonlinear dynamic behaviors of a rod fastening rotor supported by fixed-tilting pad journal bearings. *Chaos Solitons Fractals* **2014**, *69*, 129–150. [CrossRef]
2. Varela, A.; Santos, I. Stability analysis of an industrial gas compressor supported by tilting-pad bearings under different lubrication regimes. *ASME J. Eng. Gas Turbines Power* **2012**, *134*, 022504. [CrossRef]
3. Buchhorn, N.; Stottrop, M.; Bender, B. Influence of Active Cooling at the Trailing Edge on the Thermal Behavior of a Tilting-Pad Journal Bearing. *Lubricants* **2021**, *9*, 26. [CrossRef]
4. Xie, Z.; Rao, Z.; Liu, H. Effect of Surface Topography and Structural Parameters on the Lubrication Performance of a Water-Lubricated Bearing: Theoretical and Experimental Study. *Coatings* **2019**, *9*, 23. [CrossRef]
5. Mehdi, S.M.; Kim, T.H. Computational Model Development for Hybrid Tilting Pad Journal Bearings Lubricated with Supercritical Carbon Dioxide. *Appl. Sci.* **2022**, *12*, 1320. [CrossRef]
6. Xu, J.; Chen, R.; Hong, H.; Yuan, X.; Zhang, C. Static characteristics of high-temperature superconductor and hydrodynamic fluid-film compound bearing for rocket engine. *IEEE Trans. Appl. Supercond.* **2015**, *25*, 3601908. [CrossRef]
7. Ali, A.; Si, Q.; Wang, B.; Yuan, J.; Wang, P.; Rasool, G.; Shokrian, A.; Ali, A.; Zaman, M.A. Comparison of empirical models using experimental results of electrical submersible pump under two-phase flow: Numerical and empirical model validation. *Phys. Scr.* **2022**, *97*, 065209. [CrossRef]
8. Ali, A.; Yuan, J.; Deng, F.; Wang, B.; Liu, L.; Si, Q.; Buttar, N.A. Research Progress and Prospects of Multi-Stage Centrifugal Pump Capability for Handling Gas–Liquid Multiphase Flow: Comparison and Empirical Model Validation. *Energies* **2021**, *14*, 896. [CrossRef]
9. Bi, C.; Han, D.; Wu, Y.; Li, Y.; Yang, J. Thermohydrodynamic investigation for supercritical carbon dioxide high speed tilting pad bearings considering turbulence and real gas effect. *Phys. Fluids* **2021**, *33*, 125114. [CrossRef]
10. Qin, Z.; Han, Q.; Chu, F. Bolt loosening at rotating joint interface and its influence on rotor dynamics. *Eng. Fail. Anal.* **2016**, *59*, 456–466. [CrossRef]
11. Han, D.; Bi, C.; Yang, J. Nonlinear dynamic behavior research on high-speed turbo-expander refrigerator rotor. *Eng. Fail. Anal.* **2019**, *96*, 484–495. [CrossRef]
12. Lund, J.W. Spring and Damping Coefficients for the Tilting-Pad Journal Bearing. *Tribol. Trans.* **1964**, *7*, 342–352. [CrossRef]
13. Barrett, L.E.; Allaire, P.E.; Wilson, B.W. The Eigenvalue Dependence of Reduced Tilting Pad Bearing Stiffness and Damping Coefficients. *Tribol. Trans.* **1988**, *31*, 411–419. [CrossRef]
14. Suh, J.; Kim, C.; Han, J.H. Effffect of Thermal Boundary Condition on Tilting Pad Journal Bearing Behavior. *Appl. Sci.* **2020**, *10*, 7540. [CrossRef]
15. Ciulli, E.; Ferraro, R.; Forte, P.; Innocenti, A.; Nuti, M. Experimental Characterization of Large Turbomachinery Tilting Pad Journal Bearings. *Machines* **2021**, *9*, 273. [CrossRef]

16. Yang, L.; Qi, S.; Yu, L. Analysis on Dynamic Performance of Hydrodynamic Tilting-Pad Gas Bearings Using Partial Derivative Method. *ASME J. Tribol.* **2009**, *131*, 011703.
17. Schüler, E.; Berner, O. Improvement of Tilting-Pad Journal Bearing Operating Characteristics by Application of Eddy Grooves. *Lubricants* **2021**, *9*, 18. [CrossRef]
18. White, M.F.; Chan, S.H. The Subsynchronous Dynamic Behavior of Tilting-Pad Journal Bearings. *ASME J. Tribol.* **1992**, *114*, 167–173. [CrossRef]
19. Dousti, S.; Allaire, P. A thermohydrodynamic approach for single-film and double-film floating disk fixed thrust bearings verified with experiment. *Tribol. Int.* **2019**, *140*, 105858. [CrossRef]
20. Lv, F.; Shangguan, Y.; Zou, D.; Ji, A. Transient mixed-lubrication analysis of low-viscosity lubricated bearings under impact load with consideration of turbulence. *Phys. Fluids* **2022**, *34*, 033108. [CrossRef]
21. Yan, R.; Chen, H.; Zhang, W.; Hong, X.; Bao, X.; Ding, X. Calculation and verification of flow field in supercritical carbon dioxide dry gas seal based on turbulent adiabatic flow model. *Tribol. Int.* **2022**, *165*, 107275. [CrossRef]
22. Guenat, E.; Schiffmann, J. Real-gas effects on aerodynamic bearings. *Tribol. Int.* **2018**, *120*, 358–368. [CrossRef]
23. Bi, C.; Han, D.; Yang, J. The frequency perturbation method for predicting dynamic coefficients of supercritical carbon dioxide lubricated bearings. *Tribol. Int.* **2020**, *146*, 106256. [CrossRef]
24. Ng, C.W.; Pan, C.H.T. A linearized turbulent lubrication theory. *J. Basic Eng.* **1965**, *87*, 675–682. [CrossRef]
25. Someya, T. *Journal-Bearing Databook*; Springer: Berlin/Heidelberg, Germany, 1989.
26. Barus, C. Isothermals, isopiestics, and isometrics relative to viscosity. *Am. J. Sci.* **1893**, *45*, 87–96. [CrossRef]
27. Gao, J.; Liu, J.; Yue, H.; Zhao, Y.; Tlili, I.; Karimipour, A. Effects of various temperature and pressure initial conditions to predict the thermal conductivity and phase alteration duration of water based carbon hybrid nanofluids via MD approach. *J. Mol. Liq.* **2022**, *351*, 118654. [CrossRef]
28. Wu, Y.; Yang, L.; Xu, T.; Wu, W. Thermo-Elasto-Hydrodynamic Characteristics Analysis of Journal Microbearing Lubricated with Rarefied Gas. *Micromachines* **2020**, *11*, 955. [CrossRef]
29. Griffini, D.; Salvadori, S.; Martelli, F. Thermo-Hydrodynamic Analysis of Plain and Tilting Pad Bearings. *Energy Procedia* **2016**, *101*, 2–9. [CrossRef]
30. Ramadan, K.M.; Qisieh, O.; Tlili, I. Thermal creep effects on fluid flow and heat transfer in a microchannel gas cooling. *Proc. Inst. Mech. Eng. Part C J. Mech. Eng. Sci.* **2022**, *236*, 5033–5047. [CrossRef]
31. Nicholas, J. Tilting Pad Bearing Design. In Proceedings of the 23rd Turbomachinery Symposium, College Station, TX, USA, 13–15 September 1994; pp. 179–194.
32. Jeung, S.H.; Suh, J.; Yoon, H.S. Performance of Tilting Pad Journal Bearings with the Same Sommerfeld Number. *Appl. Sci.* **2020**, *10*, 3529. [CrossRef]
33. Dyrobes BePerf (Bearings). Available online: https://dyrobes.com/features/bearings/ (accessed on 16 May 2022).